ANNUAL REVIEWS

Annual Review of Earth and Planetary Sciences

Interface Kinetics, Grain-Scale Deformation, and Polymorphism

S.J.S. Morris

Department of Mechanical Engineering, University of California, Berkeley, California 94720; email: morris@berkeley.edu

Annu. Rev. Earth Planet. Sci. 2017. 45:245–69

The *Annual Review of Earth and Planetary Sciences* is online at earth.annualreviews.org

https://doi.org/10.1146/annurev-earth-040610-133511

Keywords

mixed-phase region, coherent and incoherent interfaces, olivine–spinel

Abstract

Deviatoric stress generated within subducting slabs by the olivine–spinel transformation has been modeled by assuming the phases to be simply connected rather than comprising a mixture in which one phase is embedded within another. Here, we use a simplified model to explain how transformation strain is incorporated into a continuum model, and we then use the simplified model to explain quantitatively the origin of the unreasonably large deviatoric stresses predicted by existing slab models. We review experiments on the transformation of single-crystal samples and argue that they are consistent with the occurrence, at the grain scale, of deviatoric stresses comparable with those predicted (erroneously) to exist at the slab scale by those slab models. Using a simple example, we show that although large deviatoric stresses can exist at the grain scale, their average over a sample containing many grains can be hydrostatic. This leads us to the problem of modeling the microscale structure. We outline the thermodynamics needed for such nonhydrostatic systems, and we illustrate their use and implications with examples.

1. INTRODUCTION

A crystalline solid can generally exist stably in more than one form (or phase), the stable lattice being determined by conditions of temperature and pressure: Diamond and graphite, as well as the various phases of ice and of silica, are examples. Here, we consider transformations that are heterogeneous: At a given time, a sample in the process of transforming can be divided into subregions, some of which have transformed and others not. Because the lattices differ between these subregions, strains develop within the transforming solid. In geodynamics, it has been assumed implicitly that the corresponding small-scale stress field is unimportant on the timescale of mantle convection and that, to the extent transformation kinetics are of interest, they can be studied by means of experiments in which the effects of the small-scale stress would, in any case, be minimal; for discussion, see Ringwood & Major (1970, section 3.3), Ringwood (1972, p. 237), and Rubie (1993, p. 252). The results of these kinetics experiments are used to estimate the depth to which the low-pressure phase olivine can persist in cold subducting slabs (e.g., Sung & Burns 1976, Rubie & Ross 1994, Devaux et al. 1997, Mosenfelder et al. 2001, Kubo et al. 2009). As discussed by, e.g., Frohlich (2006), the occurrence of deep earthquakes within a slab might be explained by the persistence within the slab of a wedge of metastable olivine which, owing to the thermally activated kinetics, could transform rapidly once sufficiently hot. The conceptual problem is then to find a mechanism allowing faulting when the deviatoric stress is small compared with the pressure; as discussed by Schubnel et al. (2013), transformational faulting is a possible mechanism.

When the problem is formulated as one of the existence of a metastable wedge, emphasis is placed on the kinetics of the transformation; none of the studies cited above attempts to calculate the stress field within the slab itself. Schubert and coworkers (Devaux et al. 2000; Guest et al. 2003, 2004), by contrast, model the stress field induced within the slab by the olivine–spinel series of transformations. To emphasize that the volume change occurring on transformation induces large stresses (even in the absence of kinetic delays), Guest et al. (2003) assume transformation to occur at thermodynamic equilibrium. In that model, deviatoric stress is generated by two transformations (olivine–modified spinel–spinel); with increasing depth, it is relaxed at a rate controlled by the nonlinear rheology of the slab. Guest et al. (2004) subsequently included interface kinetics. In both cases, the deviatoric stress is large; within a slab, stresses of ∼1 GPa are predicted to occur at depths of ∼700 km. Guest et al. (2004, p. 265) conclude that "model shear stresses seem to be too high in comparison with the assumed strength of the lithosphere," and suggest that deviatoric stress might be decreased, "for example, by considering complex mineralogy, water content, etc." We argue here that overprediction of deviatoric stress is a consequence of the implicit assumption in those studies that the phases are not dispersed, but continuous.

In Section 2, we discuss the formulation of constitutive relations appropriate to a material undergoing polymorphism. In Section 3, as an example, we discuss a model problem posed by Guest et al. (2003). Using the solution to the model problem, we point out that, for an elastic slab, the stress field induced by the transformation extends above and below the transition depth by a distance of the order of the slab thickness. Creep appears to decrease the magnitude of the shear stress but to increase the distance over which the stress is nonzero. We then use a simple example to argue that, when the phases are dispersed, the large stresses generated along phase interfaces during transformation average over many crystal grains to give smaller mean stresses. The need to resolve that internal structure provides one reason for studying the topic of this review.

Because the solutions of Guest et al. (2003, 2004) predict that, for any realistic distribution of effective viscosity, deviatoric stresses on the order of a gigapascal are generated by phase transformation, in Section 4 we review experiments demonstrating the existence of such stresses at the grain scale. Because such grain-scale stresses alter the coexistence condition for the phases,

in Section 5 we discuss thermodynamics and interface kinetics in the presence of nonhydrostatic stress. In Section 6, we introduce the distinction between coherent and incoherent interfaces and explain its implications for the thermodynamics.

In Section 7, to illustrate the preceding discussion and the implications of the constitutive relation posed in Section 2, we consider two models of phase transformation in which the phases form a composite sphere: (*a*) the product occupies the central sphere and grows into a spherical annulus of the parent (Lifshitz & Gulida 1952, Truskinovskiy 1984b, Roitburd & Temkin 1986); (*b*) the product occupies the outer rim and grows into the central sphere of the parent (Morris 2014). As in the experiments reviewed in Section 4, a uniform pressure is applied to the outer surface of the sample. We show that, because these models correctly treat the physical issues identified in Sections 2 and 5, the chief conclusions are insensitive to configuration. In particular, within a certain range of applied pressure, no transformation is possible in an elastic body; outside that range, the sample transforms at a rate controlled by interface kinetics. Experiments by Du Frane et al. (2013) on nominally anhydrous (<6 ppmw) olivine were performed at sufficiently large applied pressures that, if the material properties entering into the interface kinetics were independent of time, the sample would have transformed completely. Instead, Du Frane et al. found an extremely thin and apparently stationary rim of high-pressure phase. The inconsistency between theory and observation leads us to consider the effect of water on the rate constant.

In Section 8, we return to the concept of the incoherent interface. We argue that if, as a material element crosses the phase interface, the lattice is completely reconstructed, all record of strain occurring prior to, or during, transformation should be eliminated. In an elastic body, therefore, deviatoric stress within the product should vanish at the phase interface; elsewhere within the product, deviatoric stress in a material element should depend only on the deviatoric strain experienced by that element since its transformation. We summarize the analysis of Morris (2017), showing that, according to this model of an elastic body, if the applied pressure p_a exceeds the Clapeyron pressure $\bar{p}$, the rim thickness increases with time, but ultimately reaches a steady value that is itself a continuous function of $p_a - \bar{p}$. Unlike the model discussed above, this one does not predict a complete transformation for the conditions in the experiments of Du Frane et al. (2013); however, it predicts a much thicker rim than is observed. Both models are therefore consistent in suggesting that interface kinetics may, at least in nominally anhydrous samples, be important in limiting rim growth.

The models described in Sections 7 and 8 provide the second reason for studying the topic of this review: The magnitude of the small-scale stress field depends on the nature of the phase interface, and spatial averaging of that small-scale stress field determines the tectonic-scale stress field. Moreover, the models discussed above suggest that water has a significant effect on interface kinetics; through that effect, it could influence the small-scale stress field.

We outline the kinetic model used to fit experiments on polycrystals and to extrapolate the results to geophysical conditions. The model is geometric. It is assumed that, for constant experimental conditions, spheres of product nucleate at a constant rate $\dot{N}$ and that, following the nucleation of a sphere, the radius of the sphere increases with a constant speed c. Under these assumptions, grains that nucleated at different times must eventually overlap, and new grains of product must eventually nucleate within the transformed material. The problem of correcting for these effects was solved first, in the context of homogeneous nucleation of crystals within a melt, by Kolmogorov (1937). The model was later extended to cover the case in which product nucleates only on the faces of crystal grains. Using that form, Rubie et al. (1990) fit their experiments on the olivine–spinel transformation in Ni_2SiO_4, thereby determining values of $\dot{N}$ and c at the experimental temperature and pressure. By repeating experiments at different temperatures, one can determine the activation energy and other constants entering into the reaction kinetics.

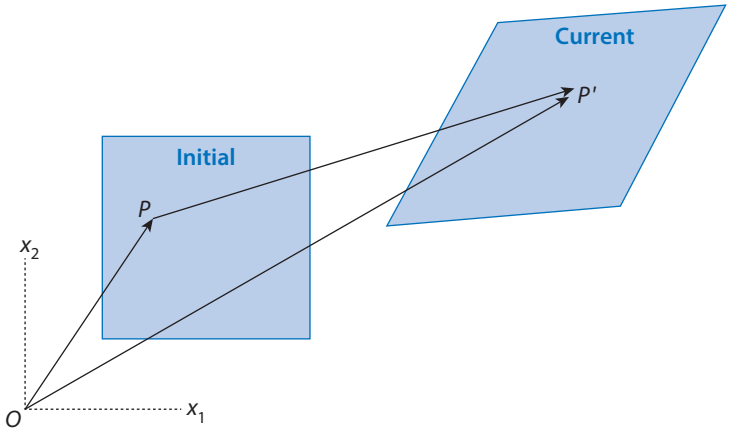

Figure 1

Initial and current state of a body undergoing polymorphic change.

2. CONSTITUTIVE RELATIONS AND POLYMORPHISM

Using examples from the literature, we show how transformation strain and creep have, so far, been included in the constitutive relation for the bulk phases. For the phase interface itself, a separate constitutive assumption is necessary, and we discuss it in Section 5.

For simplicity, we assume infinitesimal strain. We use suffix notation: $\{x_1, x_2, x_3\}$ correspond to $\{x, y, z\}$. Roman suffixes run from 1 to 3; Greek, from 1 to 2 only. We use the summation convention. For the stress tensor σ_{ij}, we use the sign convention most usual in mechanics: Tensile stresses are positive. The unit tensor is represented by δ_{ij}.

Figure 1 shows the initial and current states of a body. In the initial state, the entire body consists of phase A at a uniform pressure p_0, and the material element of interest is at point P. In the current state, that material element has moved to P'; the components of its displacement $P'P$ are denoted by u_i. As is usual in the theory of infinitesimal strain, the strain tensor e_{ij} is defined in terms of u_i by

$$2e_{ij} = \frac{\partial u_i}{\partial x_j} + \frac{\partial u_j}{\partial x_i}. \tag{1}$$

We note that e_{ij} is calculated using the entire displacement u_i of the material element from its initial position; phase does not enter into this part of the calculation.

2.1. Polymorphism with Reversible Shape Change: Model Constitutive Relation

We first treat the case in which a given material element consists either of pure phase A or of pure phase B. To specify the phase, we introduce an indicator function: $\xi = 0$ if the material element consists of A, and otherwise $\xi = 1$. For simplicity, we take the phases to be isotropic and linearly elastic; to emphasize this limitation, we use the word "model" in the heading above.

There are two contributions to the stress tensor: the hydrostatic stress $-p_0\delta_{ij}$ in the initial state and an additional contribution σ_{ij} that causes deformation from that state. We refer to σ_{ij} as the reduced stress tensor. Rather than verbally describing the characteristics of a particular type of transformation, we pose a constitutive equation and then describe the behavior of the material to which it corresponds. Following Eshelby (1961), we suppose that e_{ij} is given in terms of the

reduced stress tensor σ_{ij} as follows:

$$e_{ij} - \xi\, e^{\mathrm{T}}_{ij} = \frac{1}{2\mu}\left(\sigma_{ij} - \frac{\nu}{\nu+1}\sigma_{kk}\delta_{ij}\right). \tag{2}$$

In Equation 2, ν and μ denote the Poisson ratio and the rigidity (shear modulus). The tensor e^{T}_{ij} is a constant characteristic of the transformation; it is variously called the transformation, stress-free, or Bain strain. Equation 2 is equivalent to equations 2.18 and 2.19 of Eshelby (1961); in the Eshelby problem, the product occupies the inclusion, and the transformation strain is subtracted from the strain in the inclusion; this is consistent with Equation 2.

According to Equation 2, at a given instant, the strain is uniquely determined by the state of the material as specified by the phase ξ and the components of the stress tensor. Thus, Equation 2 describes a transformation that has the property that the strain is reversible: A body having a given initial shape can be returned to that shape by reversing the transformation, and the stress. To be definite, let $\sigma_{ij} = 0$; the stress is currently identical to that in the initial hydrostatic state. In this case, we see that $e_{ij} = \xi\, e^{\mathrm{T}}_{ij}$. If $\xi = 0$, so that the material element currently consists of the same phase A as in its initial state, then the strain is zero. The state $\xi = 0$ could occur if the element had never changed phase at all, or if it had changed to phase B and then subsequently changed back to phase A. Similarly, if $\xi = 1$, so that the element has changed phase (any odd number of times), the strain tensor is given by e^{T}_{ij}. Of course, although $\sigma_{ij} = 0$ in the current state, at some time between the initial and current states the element has been subject to stress that induced the phase change. This confirms that Equation 2 describes a transformation producing a reversible change of shape: The change of shape is specified by the tensor e^{T}_{ij}. James & Hane (2000) and Bhattacharya (2003) give the components of e^{T}_{ij} for transformations between specific crystal lattices.

To a first approximation, when silica converts from its low quartz to its high quartz polymorph, the shape change is reversible, as Le Chatelier (1890) and Mallard & Le Chatelier (1890) write in describing its discovery:

> At a temperature of about 570 °C, this substance undergoes a reversible change of state . . . . This change of state has the notable property of leaving the crystal lattice intact, and, thus, of not affecting even such a remarkable property as rotatory polarization [Mallard & Le Chatelier 1890, p. 123]. The same phenomenon always occurs each time the critical temperature is reached, either from below or from above [Le Chatelier 1890, p. 119].

Dolino (1990) and Heaney & Veblen (1991) give more complete descriptions of this transition; James (1986) gives the components of e^{T}_{ij}.

Equation 2 is analogous to the Duhamel–Neumann constitutive relation for thermoelasticity, as given by Sokolnikoff (1956, p. 359). Eshelby (1961, p. 92) points out the analogy between his problem and that of thermal stresses: Thermoelastic strain is reversible in the sense that we apply to Equation 2, and the displacement field is continuous. Eshelby (1961, p. 91) emphasizes that his analysis applies provided that "the inclusion is 'bonded' to the matrix before, during and after the transformation." Stresses induced by volume change also occur in the process of metamictization, i.e., structural change induced within a crystal by radioactive decay of atoms within the structure. In that context, Lee & Tromp (1995, equation 24) formulate a constitutive equation equivalent to Equation 2 and use it to predict stresses developed when metamictization occurs either as a central core or as a rim. Of course, in metamictization, the interface between altered and unaltered lattices does not propagate through the mineral; in this, the process differs from a phase change.

As for the olivine–spinel transformation, if the stress applied to the sample is sufficiently close to hydrostatic, then only the volume change is reversible (Vaughan et al. 1982, 1984; Green 1986; Green et al. 1992). The transformation has been modeled using Equation 2 with $e_{ij}^{\mathrm{T}} = \frac{1}{3}\theta_0\delta_{ij}$, where $\theta_0 = (V_0^{\mathrm{B}} - V_0^{\mathrm{A}})/V_0^{\mathrm{A}}$ is the fractional change in specific volume. In this context, Equation 2 has the advantage of stating explicitly that e_{ij}^{T} enters through the constitutive relation for the product phase, not through that for the parent: When modeling growth of a spinel rim on a particle of olivine, e_{ij}^{T} must be subtracted from the strain in the rim, not from that in the parent olivine. Although, with hindsight, this is obvious, Morris (2014, appendix) has shown that early attempts to model rim growth incorrectly include transformation strain.

There is, however, something troubling about using Equation 2 to describe a transformation in which only the volume change is reversible. Equation 2 relates the strain experienced by a material element as a result of its displacement from the initial state to its current state. According to Equation 2, if the element changes phase during that displacement, the total strain is unchanged, apart from the reversible dilatation associated with the transformation: Almost all the strain experienced by the material element during its existence in the initial phase is retained despite the reorganization of the crystal lattice that occurs during transformation. As we discuss further in Section 7, although it is self-consistent to use Equation 2 with $e_{ij}^{\mathrm{T}} = \frac{1}{3}\theta_0\,\delta_{ij}$, the resulting model may not describe the physical process correctly.

2.2. Modeling Transformation Strain at the Tectonic Scale

Kirby et al. (1996, p. 286) draw an analogy between thermoelasticity and the generation of stress within a subducting slab owing to the volume change in the olivine–spinel transformation. The analogy is developed by Schubert and coworkers (Devaux et al. 2000; Guest et al. 2003, 2004): It is assumed (implicitly) that within a region of mixed phase, both phases are at the same pressure p and temperature T. Let the densities of the phases be $\rho_{\mathrm{A}}(p, T)$ and $\rho_{\mathrm{B}}(p, T)$ and let the volume fraction of phase B be ξ. Then, denoting the mixture density by ρ, we have $\rho = (1-\xi)\rho_{\mathrm{A}}(p, T) + \xi\rho_{\mathrm{B}}(p, T)$ (as in Devaux et al. 2000, equation 21). Expanding this expression to first order in a Taylor series in p and T (but not in ξ) about the reference state p_0, T_0, in which $\rho = \rho_{\mathrm{A}}(p_0, T_0)$, we find that

$$\frac{\rho}{\rho_{\mathrm{A0}}} - 1 = -\xi\theta_0 + (p - p_0)\kappa_0 - (T - T_0)\alpha_0;$$

as defined above,

$$\theta_0 = (V_0^{\mathrm{B}} - V_0^{\mathrm{A}})/V_0^{\mathrm{A}}.$$

The mixture compressibility is $\kappa_0 = (1-\xi)\kappa_{\mathrm{A0}} + \xi\kappa_{\mathrm{B0}}$, and likewise for the mixture expansivity α_0; these equations are special cases of equation 21 of Devaux et al. (2000). Compressibility and expansivity are as defined by Pippard (1957, p. 61). Using the relations $e_{kk} = 1 - \rho/\rho_{\mathrm{A0}}$ and $p - p_0 = -\frac{1}{3}\sigma_{kk}$, we obtain the linearized equation of state:

$$e_{kk} = \tfrac{1}{3}\kappa_0\,\sigma_{kk} + \alpha_0\,(T - T_0) + \xi\theta_0. \tag{3a}$$

For $T = T_0$ and $e_{ij}^{\mathrm{T}} = \frac{1}{3}\theta_0\delta_{ij}$, Equation 3a reduces to the dilatational part of Equation 2, with ξ then being either zero or unity. We note that the form of Equation 3a is consistent with subtracting transformation strain from strain in the product, but not in the parent.

For the deviatoric components, Schubert and coworkers (Devaux et al. 2000; Guest et al. 2003, 2004) take the slab material to behave as a Maxwell body. That constitutive relation is stated for a material that is stationary relative to the laboratory; application to the slab is covered in Section 3. For infinitesimal strain, the deviatoric strain tensor $e'_{ij} = e_{ij} - \frac{1}{3}e_{kk}\delta_{ij}$ is related to the deviatoric

stress tensor $\sigma'_{ij} = \sigma_{ij} - \frac{1}{3}\sigma_{kk}\delta_{ij}$ as follows:

$$2\mu \frac{\partial e'_{ij}}{\partial t} = \frac{\partial \sigma'_{ij}}{\partial t} + \frac{\mu}{\eta}\sigma'_{ij}; \tag{3b}$$

here, μ and η denote respectively the volume-weighted average of the rigidities and of the effective viscosities of the separate phases, as given by equation 21 of Devaux et al. (2000). Apart from that modification of μ and η, Equation 3b is identical to the corresponding expression for a single-phase Maxwell body.

Although it is consistent with the use of the geometric model of kinetics to predict the volume fraction of product, the assumption, implicit in Equations 3a and 3b, that both phases are at common pressure is not trivial. In Section 4, we discuss experimental evidence suggesting the existence of large pressure gradients at the grain scale. In Section 3, we discuss why that assumption may lead to the prediction of an unreasonably large macroscopic stress.

3. EXAMPLE: TRANSFORMATION STRESS IN A SUBDUCTING SLAB

Figure 2*a* shows the test problem formulated by Guest et al. (2003) as part of their analysis of the stress induced within a subducting slab by the olivine–post-spinel series of transformations. To explain the behavior found in their detailed simulations, the authors consider a simplified model, retaining only the essential feature of the volume change due to transformation. The following assumptions are made: The slab descends vertically; mantle density is uniform; buoyancy is negligible; transformation occurs at thermodynamic equilibrium; the latent heat of transformation is zero; the temperature is uniform; and the viscosity of the surrounding mantle is negligibly small compared with that of the slab, so that on the slab sides and tip, the mantle imposes a hydrostatic pressure increasing linearly with depth. The slab material undergoes a single transformation from phase A to phase B at a pressure existing within the surrounding mantle at a depth indicated, in **Figure 2*a***, by the horizontal broken line. Because it clarifies the mechanism by which deviatoric

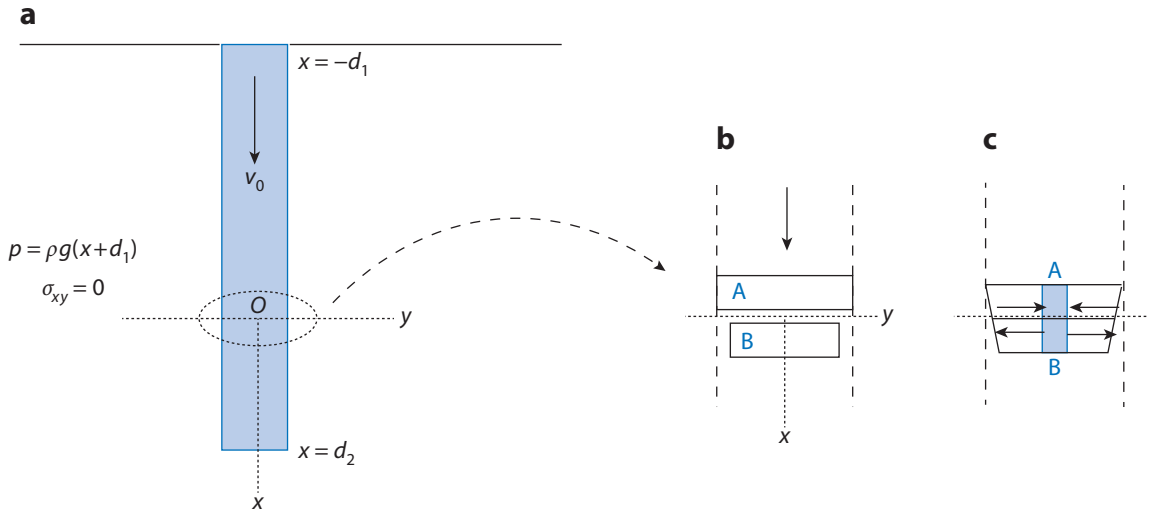

Figure 2

(*a*) Geometry of the test problem. (*b*,*c*) Relation between deviatoric stress and volume change. (*b*) Perfect slip: no deviatoric stress. (*c*) Continuous displacement: Arrows show the normal stress σ_{yy} required on the faces of the shaded rectangle for the displacement to be continuous across the interface at $x = 0$.

stress is generated, and the scale on which it decreases, we carefully discuss this simplified problem, assuming elasticity. Creep modifies the stress field, but does not alter the generation mechanism.

In **Figure 2*a***, the coordinate origin O is at the transition depth; x_1 increases downward; x_2 increases across the thin dimension of the slab; and x_3 is directed out of the page. For brevity, we call x_3 the trenchwise direction. Where convenient, $\{x_1, x_2, x_3\} = \{x, y, z\}$.

Figure 2*b*,*c* is used to explain how deviatoric stress arises in the test problem. Suppose the phases are free to slip along the phase interface at $x = 0$, as in **Figure 2*b***. Because the interface is assumed to be flat, transformation can then occur without causing deviatoric stress. Removing the resulting discontinuity in displacement requires column B to be stretched and column A to be compressed, as in **Figure 2*c***. Continuity of the displacement vector therefore requires the component σ_{22} of the stress tensor to be discontinuous in an elastic body, and likewise for σ_{33}. Because, as shown in **Figure 2*a***, the outer ends of each column are subject to the same pure pressure, the discontinuity in σ_{22} is, of course, not due to an external applied force. Rather, being in compression, column A tends to pull column B outward; column B, being in tension, tends to pull column A inward. We note that this stress state is consistent with the balance of linear momentum, which requires only that σ_{11}, σ_{12}, and σ_{13} each be continuous across the plane $x = 0$. This argument is formalized below.

For any property f, the notation $[f]_{\mathrm{A}}^{\mathrm{B}}$ represents the difference between the value taken by f on the B side of the interface and the value taken on the A side.

The magnitude of $[\sigma_{22}]_{\mathrm{A}}^{\mathrm{B}}$ sets the scale for deviatoric stress. To determine it, we use the constitutive equation and the condition that the displacement vector be continuous. Initially, in the model problem, a material element is in phase A at uniform hydrostatic pressure far above the transition depth. As the material element descends, it suffers a deformation that can be resolved into two parts: an isotropic contraction caused by the background hydrostatic stress and a deformation caused by the stress resulting from the phase change. Assuming that the strain in the second part is infinitesimal, Guest et al. (2003) (implicitly) invoke the principle of superposition and solve a boundary-value problem for it. For this component, the initial (reference) state is one of zero strain and stress.

Let σ_{ij} denote the reduced stress tensor, i.e., the difference between the total stress and the hydrostatic stress $\sigma_{ij} = -\rho g(x + d_1)\delta_{ij}$ applied by the mantle to the slab. If there were no phase change, an element of the slab would translate with the uniform speed v_0 of the slab. For the geometry shown in **Figure 2**, at time t, an element whose initial position was a_i would be at position $x_i = a_i + v_0\delta_{i1}\,t$ at time t. The displacement u_i introduced by Devaux et al. (2000, equation 4) is defined (here) by $x_i = a_i + v_0\delta_{i1}t + u_i$; here u_i is the displacement of the element from the position it would have if there were no phase change.

We show that the magnitude of the deviatoric stress can be determined directly from the constitutive equation and the condition that displacements be continuous across the interface. Because u_i is continuous across the interface, $[e_{22}]_{\mathrm{A}}^{\mathrm{B}} = 0 = [e_{33}]_{\mathrm{A}}^{\mathrm{B}}$. Applying these conditions to Hooke's law (Equation 2), we obtain two simultaneous equations for the unknowns $[\sigma_{22}]_{\mathrm{A}}^{\mathrm{B}}$, $[\sigma_{33}]_{\mathrm{A}}^{\mathrm{B}}$:

$$0 = \frac{1}{3}\mu\theta_0 + [\sigma_{22}]_{\mathrm{A}}^{\mathrm{B}} - \frac{\nu}{1+\nu}[\sigma_{22} + \sigma_{33}]_{\mathrm{A}}^{\mathrm{B}}, \tag{4a}$$

$$0 = \frac{1}{3}\mu\theta_0 + [\sigma_{33}]_{\mathrm{A}}^{\mathrm{B}} - \frac{\nu}{1+\nu}[\sigma_{22} + \sigma_{33}]_{\mathrm{A}}^{\mathrm{B}}. \tag{4b}$$

The expression $[\sigma_{11}]_{\mathrm{A}}^{\mathrm{B}} = 0$ has been used. By solving Equation 4b, we obtain

$$[\sigma_{22}]_{\mathrm{A}}^{\mathrm{B}} = [\sigma_{33}]_{\mathrm{A}}^{\mathrm{B}} = -\frac{2}{3}\mu\frac{1+\nu}{1-\nu}\theta_0. \tag{5}$$

Equation 5 is a property of the phase transformation; it holds only if $[u_2]_A^B = 0 = [u_3]_A^B$. For the olivine–post-spinel series of transformations, $\theta_0 < 0$; according to Equation 5, both components of normal stress transverse to the slab increase across the phase interface.

For $\mu = 100$ GPa, $|\theta_0| = 0.06$, and a Poisson ratio of $\nu = \frac{1}{4}$, the stress jump predicted by Equation 5 is ~7 GPa. Guest et al. (2003, figure 5*e*) show the stress distribution for their test problem. Although that calculation is for a Maxwell body, the viscosity of 10^{29} Pa · s is sufficiently large for the response to be effectively elastic (Guest et al. 2003, ¶38). Owing to a different choice of coordinates, their σ_{11} corresponds to our σ_{22} and vice versa. According to their figure, the jump in σ_{33} (measured from peak to peak) is 2.1 GPa; the jump in their σ_{11} (also from peak to peak) is 1.7 GPa (~20% smaller than that in σ_{33}). Their values are about one-third those predicted by Equation 5.

As noted by Kirby et al. (1996, p. 262), it has been argued that deep earthquakes could not be caused by metastable phase changes because the source mechanism is consistent with failure under shear rather than with implosion. The virtue of the model of Guest et al. (2003) is in demonstrating that volume reduction generates shear stress. This large shear stress could be relaxed by creep or by faulting, raising the issue of why faulting should occur far below the location of the maximum stress.

Guest et al. (2003) model the stress field in a subducting slab in two cases: plane deformation (the component u_3 of displacement along the trench axis is taken as zero) and a version of plane stress in which the trenchwise stress component σ_{33} is taken as zero. But, because their form of the plane stress assumption cannot satisfy both members of Equation 4, it seems that, whenever conditions are such that the material behaves elastically at the interface, at least one component of the displacement vector must be discontinuous in their plane stress solutions.

We consider only plane deformation. For it, $u_3 = 0$ and $\partial/\partial x_3 = 0$; so $0 = e_{31} = e_{32} = e_{33}$. Substituting $e_{33} = 0$ into Equation 2, we obtain

$$\sigma_{33} = \nu\sigma_{\lambda\lambda} - \frac{2}{3}\mu(1+\nu)\xi\theta_0. \tag{6}$$

We eliminate σ_{33} between Equations 2 and 6:

$$e_{\alpha\beta} = \frac{1}{3}(1+\nu)\theta_0\xi\,\delta_{\alpha\beta} + \frac{1}{2\mu}(\sigma_{\alpha\beta} - \nu\sigma_{\lambda\lambda}\,\delta_{\alpha\beta}). \tag{7}$$

To obtain the factors determining the magnitude of the stress, and the length scale on which it varies, we formulate the boundary-value problem for it. Although σ_{33} is nonzero for plane deformation, it is independent of x_3. Consequently, when expressed in terms of the reduced stress tensor, the conditions of equilibrium become $\partial\sigma_{\alpha\beta}/\partial x_\beta = 0$. They are satisfied identically by introducing the stress function χ, defined thus:

$$\sigma_{xx} = \frac{\partial^2\chi}{\partial y^2}, \quad \sigma_{xy} = -\frac{\partial^2\chi}{\partial x\partial y}, \quad \sigma_{yy} = \frac{\partial^2\chi}{\partial x^2}. \tag{8a,b,c}$$

Here $\{x, y, z\} = \{x_1, x_2, x_3\}$. Substituting Equation 8 into the equation of compatibility (Fung 1965, pp. 103, 235), we find that, as in the theory of plane strain for a single phase, χ satisfies the biharmonic equation below (Equation 9a). Because that equation does not define a length scale, the reduced stress must vary with vertical distance x_1 on the single length scale imposed by the boundary conditions, i.e., the slab thickness $2a$.

Both above and below the phase interface, χ proves to approach a limiting value when $|x| \sim a$ (see Guest et al. 2003, figure 5*e*). To determine the reduced stress, we may thus take the slab to be infinite in length. For the geometry shown in **Figure 2**, but now with $-\infty < x < \infty$, χ satisfies

the following problem:

$$\text{For } |y| < a \text{ and } x \neq 0, \quad \nabla^2\nabla^2\chi = 0; \tag{9a}$$

$$\text{at } x = 0, \quad [\chi]_{\mathrm{A}}^{\mathrm{B}} = 0 = \left[\frac{\partial\chi}{\partial x}\right]_{\mathrm{A}}^{\mathrm{B}}; \tag{9b,c}$$

$$\left[\frac{\partial^2\chi}{\partial x^2}\right]_{\mathrm{A}}^{\mathrm{B}} + \frac{2}{3}\mu\frac{1+\nu}{1-\nu}\theta_0 = 0; \tag{9d}$$

$$\text{at } |y| = a, \quad \chi = 0 = \frac{\partial\chi}{\partial y}; \tag{9e,f}$$

$$\text{as } x \to \infty, \quad \chi \to 0. \tag{9g}$$

The simplified problem is now reduced to a well-known form. Similar mathematical problems describe the stress in a thin elastic plate loaded at one end, or the slow viscous flow driven by end stresses (or a thermal plume) in a cavity (see, e.g., Bloor & Wilson 2006). The jump condition (Equation 9d) explicitly displays the magnitude of the stress. The other equations are standard: Equations 9b and 9c express continuity of the stress components σ_{xx} and σ_{xy}, and Equations 9e and 9f state that the ambient mantle applies a pure hydrostatic stress to the slab tip and sides.

The problem described by Equations 9a–g is satisfied if χ is an odd function of x satisfying Equations 9a, 9e, 9f, and 9g within the half-strip $0 < x < \infty$, $|y| < a$, subject at $x = 0$ to the conditions

$$\chi = 0, \quad \frac{\partial^2\chi}{\partial x^2} + \frac{1}{3}\mu\frac{1+\nu}{1-\nu}\theta_0 = 0. \tag{10a,b}$$

For this work, the problem for the half-strip was solved by taking the Fourier sine transform, then using the residue theorem to evaluate the inversion integral.

Figure 3 shows values of $\sigma_{xx}(x, 0)$ and $\sigma_{yy}(x, 0)$ so obtained (as a function of x/a). Stress is given in a unit equalling half the jump in σ_{22} described previously:

$$\sigma_s = \frac{1}{3}\mu|\theta_0|\frac{1+\nu}{1-\nu}. \tag{11}$$

Expressed in the scales $\{\sigma_s, a\}$, Equation 10b states that $\sigma_{yy} \to -\operatorname{sgn}\theta_0$ as $x \to 0^+$; for the olivine–spinel transformation, $\theta_0 < 0$. Dimensionless stress components are independent of the rigidity μ and Poisson ratio ν. Dimensionless displacements are obtained by substituting the stress components in the dimensionless form of Hooke's law (Equation 7); these displacements necessarily depend on ν (but not on μ).

According to **Figure 3**, both σ_{xx} and σ_{yy} are positive (tensile) for $\theta_0 < 0$; the axial stress σ_{xx} has a maximum value of 0.1713, about one-fifth the maximum value of σ_{yy}. The corresponding dimensional value for the axial stress is $\sigma_{xx} \sim 0.5$ GPa for $\nu = \frac{1}{4}$, $\mu = 100$ GPa, and $\theta_0 = -0.06$. [The corresponding value estimated from figure 5*e* of Guest et al. (2003) is ∼0.2 GPa.]

For x large compared with the slab thickness, σ_{xx} and σ_{yy} both vanish, for the following reason. At the interface $x = 0$, the parent (in compression) applies to the product (in tension) a shear stress σ_{xy} that is directed outward: $\sigma_{xy} \gtrless 0$ for $y \gtrless 0$. Because the resultant shear force exerted across the interface for $0 < y < a$ is equal in magnitude, but opposite in sign, to that exerted across $-a < y < 0$, the effect of these opposing forces cancels with increasing x, and the cancellation occurs over a distance of the order of the scale on which the variation in $\sigma_{xy}(0, y)$ occurs. This is consistent with the Saint-Venant principle.

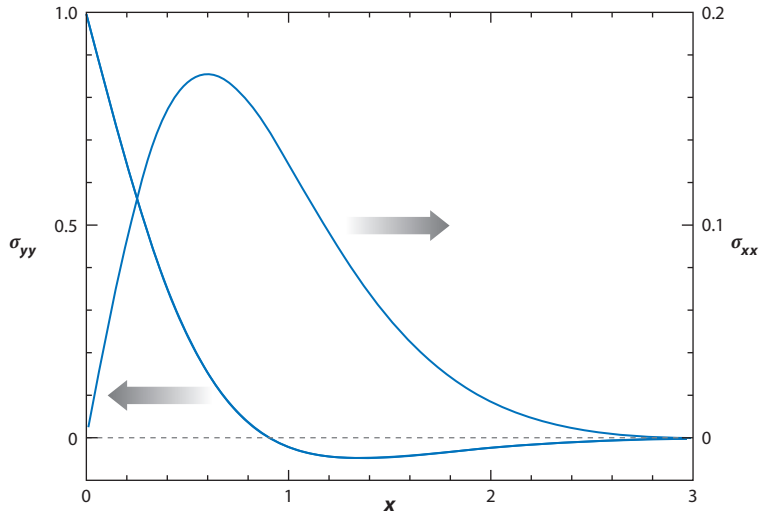

Figure 3

Dimensionless stress components σ_{xx}, σ_{yy} on the centerline $y = 0$ as functions of distance x down the slab. For the scales used to define dimensionless variables, see Equation 11.

The trenchwise stress component σ_{zz} is the largest of the three normal stresses and does not vanish with depth (in the elastic solution). Substituting the values of σ_{xx} and σ_{yy} at $x = 0$ into Equation 6 and using the identity $\text{sgn } x = 2\xi - 1$, we obtain

$$\sigma_{zz} = -\frac{1}{3}\mu\theta_0 \frac{1+\nu}{1-\nu}(1 - \nu + \text{sgn } x). \tag{12}$$

This result has implications for the phase boundary. Unlike the other nonzero components of the stress tensor, the trenchwise component σ_{zz} is neither odd nor even. Because strain energy depends on the squares of the stress components, the contributions made by σ_{xx}, σ_{yy}, and σ_{xy} are continuous across the interface. By contrast, ${\sigma_{zz}}^2$ is discontinuous. As a unit mass is transformed, its strain energy therefore increases abruptly; this increase must be balanced by power supplied by the stress. As a result, a higher pressure is required to induce the transformation: The equilibrium phase boundary is shifted downward, giving rise to metastability. In Section 7.2, we discuss the relation between strain energy and metastability in detail.

We now discuss creep. For the geometry shown in **Figure 2**, in which the slab translates in the x direction with uniform speed v_0, but in which the axes are fixed in the phase interface, partial derivatives with respect to time in the Maxwell constitutive relation (Equation 3b) are replaced by $\partial/\partial t + v_0(\partial/\partial x)$. For the cases illustrated in figure 5 of Guest et al. (2003), the tip of the slab is far below the phase interface, and the stress field is steady. Then Equation 3b becomes

$$2\mu\frac{\partial e'_{ij}}{\partial x} = \frac{\partial \sigma'_{ij}}{\partial x} + \frac{\mu}{\eta v_0}\sigma'_{ij}. \tag{13}$$

According to Equation 13, the elastic strain rate and the creep strain rate balance when the deviatoric stress varies with x on the length scale $L_s = \eta\, v_0/\mu$.

For the simplified model (**Figure 2**), Guest et al. (2003) take η to be independent of stress and temperature. Comparing their figures 5*e* (elastic) and 5*f* ($\eta = 10^{24}$ Pa · s), we see that, as in the elastic solution, the trenchwise stress component σ_{zz} rises to a maximum value; although creep barely alters the height of that maximum, it does permit σ_{zz} to relax to zero with increasing x.

According to Devaux (2000, caption to figure 5), the stress measure being graphed is the second invariant J_2' of the deviatoric stress tensor: For the plane deformation being considered here, $J_2' = \frac{1}{6}[(\sigma_{xx} - \sigma_{yy})^2 + (\sigma_{yy} - \sigma_{zz})^2 + (\sigma_{zz} - \sigma_{xx})^2] + \sigma_{xy}{}^2$ (see, e.g., Fung 1965, p. 80). Because σ_{zz} is large compared with the other stress components, graphs of shear stress in the works of Guest et al. (2003, 2004) are, roughly speaking, graphs of the trenchwise component σ_{zz}.

We have discussed the model problem illustrated in **Figure 2** with and without creep. Using the insight thus gained, we interpret the main studies by Schubert and coworkers (Devaux et al. 2000; Guest et al. 2003, 2004). In these, laboratory studies of rheology are used to define an effective viscosity for use in the Maxwell constitutive relation (Equation 3); T is predicted using the thermal model of Devaux et al. (1997), and an appropriate phase diagram is used.

Comparing the results of Guest et al. (2003) with those of Guest et al. (2004), we see that the chief conclusions are independent of interface kinetics. Having assumed thermodynamic equilibrium, Guest et al. (2003) conclude:

> Our model predicts high shear stress in the depth range 400–700 km with two maxima, one below the uppermost phase transformation . . . at 400 km depth and the other one below the phase transformation at 480 km depth [¶41]. Maximum model shear stress (1.4 GPa) . . . occurs just below the phase boundary at 480 km depth . . . . Shear stress magnitudes in the rest of the transition zone [are] 0.9–1.2 GPa for plane strain and a "cold" mantle . . . and 0.5–0.7 GPa for a "hot" mantle [¶45].

This quotation is supported by figure 10 of Guest et al. (2003), in which a tongue of deviatoric stress in the range 0.8–1 GPa extends to about 700 km.

Using their model with kinetics included, Guest et al. (2004, p. 260) reach similar conclusions: "Maximum shear stress (1–1.4 GPa) is concentrated inside the bottom part of the metastable wedge . . . in the depth range 380–430 km and along the phase boundaries . . . in the depth range 380–450 km." Guest et al. also report high shear stress in the depth range 450–640 km. In figure 4 of Guest et al. (2004) (cold mantle), a tongue of shear stress in the range 0.8–1 GPa extends to about 700 km, as in the equilibrium model of Guest et al. (2003). This suggests that the structure of the stress field is dominated by creep rather than by kinetics. We suggest that the important effect of kinetics, and the grain-scale deformation with which kinetics interact, is to set the scale for the mixed-phase region.

Physical reasoning suggests that the large deviatoric stresses predicted by the model of Guest et al. (2003, 2004) are a consequence of the topology assumed by them. Consider a sample in which transformation is driven by applying a uniform hydrostatic pressure to the sample surface. To show the effect of a phase not being simply connected, we use the simplest example, in which dense product B nucleates as isolated particles within a matrix of less-dense parent A, so that phase B is not simply connected. Because mass conservation requires each growing particle of B to incorporate mass, the ambient phase A is deformed, and the stress is locally nonhydrostatic.

The boundary condition, however, implies that the volume-averaged stress is hydrostatic. Indeed, averaged over the entire sample volume V', σ_{ik} satisfies the identity

$$\frac{1}{V'} \int_{V'} \sigma_{ik} \, \mathrm{d}V' = -p_0 \delta_{ik}. \tag{14}$$

This identity is obtained by multiplying the equation of equilibrium $\partial \sigma_{ij}/\partial x_j = 0$ by x_k, integrating, and then using the divergence theorem and the boundary condition at the sample surface (see, e.g., Hill 1963, p. 362). Physically, large deviatoric stresses on one side of a grain cancel with stresses of opposite sign on the opposite side; this cancellation occurs even if B forms as a rim on grains in a polycrystal of A.

Of course, Equation 14 also applies to the geometry of the test problem shown in **Figure 2**. In that case, Equation 14 is satisfied because, as we have seen, the stress function χ is an odd function of x but an even function of y. But, because each phase is simply connected for that geometry, Equation 14 is compatible with the occurrence of large shear stress at the scale of the entire sample.

Although, in Equation 14, V' refers to an entire sample, the same identity should apply to any subregion of a sample, provided that the sample is statistically homogeneous and the subregion is large enough to contain many grains. Seismic stress drop represents the average stress over a volume whose dimension is comparable to that of the rupture zone. That dimension is on the scale of kilometers for small earthquakes and increases with magnitude; even for the smallest earthquakes, there is a large separation of length scales between the grains and the size of the rupture zone. It seems, therefore, that one should include microstructure in models used to predict stress at tectonic scales. Doing so requires us to understand the processes operating at the grain scale.

4. EXPERIMENTS ON SINGLE CRYSTALS

The analyses of Schubert and coworkers (Devaux et al. 2000; Guest et al. 2003, 2004) predict the generation of large deviatoric stresses within a transforming solid. Laboratory experiments on the olivine–spinel transformation in single crystals demonstrate the physical existence of local stresses of comparable magnitude. In these experiments, the pressure medium was NaCl, Ag, or Au. For the purpose of such experiments, these solids are inert and soft; they do not themselves transform at the experimental pressures, and each has an athermal flow strength, i.e., a shear strength in the absence of thermal energy (Karato 2008, p. 33) that is small compared with that of olivine. Were this condition not satisfied, the loading device would apply a nonhydrostatic stress, tending to deform the sample. Even with this precaution, some recovered samples show deformation: Compare figure 2 of Du Frane et al. (2013) with figure 2 of Mosenfelder et al. (2000).

As an example of sensitivity to experimental conditions, we note that Diedrich et al. (2009, figure 11) observe some limited intracrystalline nucleation in the olivine core within their hydrated samples, but not within their nominally anhydrous samples. Du Frane et al. (2013, p. 5) note that the spectra of some hydrated samples might suggest the occurrence of intracrystalline nucleation, but add nothing more definite. By contrast, in experiments using fine-grained olivine as a pressure medium (and with, presumably, unknown water content), Kerschhofer et al. (1998, p. 625) find that in "all samples from experiments at T > 900°C intracrystalline transformation occurred in the olivine single crystals."

When water content and applied shear stress are controlled, experiments on single crystals are qualitatively consistent in showing that as the spinel rim grows into the olivine, the interface speed decreases. This decrease is not consistent with the assumptions of the geometric theory of kinetics discussed in Section 1.

Kubo et al. (1998b) transformed an ensemble consisting of 19 1-mm cubes of single-crystal $(Mg_{0.89}Fe_{0.11})_2SiO_4$ at four combinations of applied pressure and temperature. Rim thickness was measured by quenching and then sectioning the sample. Each measurement corresponded to a different sample and experiment. Kubo et al. (1998b, p. 3) and Mosenfelder et al. (2000, p. 67) report that there is no evidence for crystallographic relation between the olivine and wadsleyite phases and infer that the interface is incoherent (see Section 5). For runs at 1,303 K and 13.5 GPa and at 1,503 K and 14 GPa, Kubo et al. (1998b) followed rim growth in a series of experiments lasting 10 h. Because, in these experiments, all growth observed at 10 h had already occurred within the first 1–2 h, Kubo et al. (1998b, p. 1) conclude that "growth eventually ceased."

Dislocation densities provide the evidence for large local stresses within the rim. Kubo et al. (1998b, p. 4) report a dislocation density within the product rim of between 10^{13} and 10^{14} m^{-2}; they describe this density as being "comparable with that of β-phase [i.e., wadsleyite] deformed experimentally." We note that, although, according to Rubie et al. (1993, p. 318), preparing samples from single crystals itself induces dislocations within a distance of ∼10–20 μm from the surface, the resulting densities are about four orders of magnitude less than those seen by Kubo et al. (1998b). It can be reasonably inferred, then, that the high dislocation densities observed in the experiments of Kubo et al. (1998b) were generated within the sample by the transformation itself.

This conclusion is supported by the effect of water on the microstructure. By hydrating the pressure medium, Kubo et al. (1998a) showed that water strongly increases the interface speed in the olivine–wadsleyite transformation. At fixed temperature and pressure (1,303 K and 13.5 GPa), increasing the $Mg(OH)_2$/NaCl ratio of the pressure medium caused an increase in the water content of the wadsleyite rim, as measured[1] in recovered samples. Both dislocation density and structure were affected. At 200 ppmw of H_2O to $(Mg_{0.9}Fe_{0.1})_2SiO_4$ (olivine), dislocation density was high (at $\sim 10^{14}$ m^{-2}). The dislocations were tangled; according to Kubo et al. (1998a, p. 86), tangling implies that the wadsleyite rim has undergone strain hardening (some creep, at least, must have occurred). At 500 ppmw, dislocation density was an order of magnitude less, and the dislocations were organized into subgrains; dislocation recovery had therefore occurred, thereby facilitating creep and permitting more of the sample to transform. At 2,100 ppmw, the sample transformed completely after 3 h (Kubo et al. 1998a, figure 2). These observations show that deviatoric stress is generated within the sample by the transformation; that it impedes transformation; and that the olivine–spinel transformation is sensitive to the presence of hydrogen: 200 ppmw of H_2O corresponds to about three H atoms for every thousand Si atoms.

In a significant addition to this work, Diedrich et al. (2009) and Du Frane et al. (2013) studied the effect of water at lower concentrations. Their technique differed from that of Kubo et al. (1998a). In the experiments of Kubo et al., water was absorbed into the rim from the pressure medium during the experiment. In the more recent experiments of Diedrich et al. and Du Frane et al., the sample was hydrated in a separate experiment, and the concentration was then measured to ensure that water was uniformly distributed across the sample. This is significant because water is more soluble in the rim phase (ringwoodite in the more recent experiments) than in the parent olivine, and as the rim grows, water is drawn from the olivine core into the rim (see Diedrich et al. 2009, figure 12).

We compare figure 4*a* of Du Frane et al. (2013) with figure 6 of Kubo et al. (1998b). For the former, temperature, pressure, and bulk water content were 1,273 K, 18 GPa, and less than 6 ppmw (see Du Frane et al. 2013, table 1). For the latter, the corresponding values were 1,303 K, 13.5 GPa, and ∼200 ppmw. In both cases, rim growth appears to have ceased after ∼100 min, and the experiments were continued for a sufficiently long time to show that growth had ceased. In the experiments of Kubo et al., the final rim thickness was ∼50 μm; in that of Du Frane et al., it was only ∼10 μm. However, the potential difference driving the transformation was over 10 times greater in the experiments of Du Frane et al. than in the experiments of Kubo et al.; Mosenfelder et al. (2001, table 1) give values of the potential difference of the phases. (Owing to the difference in experimental pressures, the phases in the rim were, of course, different in the two experimental settings: The phase was wadsleyite in the experiments of Kubo et al. and

[1]This measurement was done using infrared spectroscopy. According to Karato (2008, p. 184), what is actually detected is the absorption of light of a given wavelength by a sample containing OH bonds (in any form).

ringwoodite in the experiments of Du Frane et al.) The difference suggests that nearly anhydrous ringwoodite may be significantly stronger than hydrous wadsleyite. Water might, however, affect the transformation, either by influencing the reaction rate at the phase interface or by weakening the entire rim.

These alternatives are not mutually exclusive. As shown by Kohlstedt et al. (1996), water is more soluble in the high-pressure phases, wadsleyite and ringwoodite, than in the parent olivine. Consequently, as the rim grows, water is drawn from the olivine core into the rim, as shown in figure 12 of Diedrich et al. (2009). As stated by Mosenfelder et al. (2001, p. 169) in a discussion of the experiments of Kubo et al. (1998a), "partitioning of water into the wadsleyite may promote hydrolytic weakening during the transformation, but may also result in depletion of hydrogen at the interface . . . thus slowing the growth rate."

In Section 7, we discuss the modeling of these experiments; to do so, we first need to treat thermodynamics and kinetics in the presence of deviatoric stress.

5. THERMODYNAMICS AND KINETICS

We follow Paterson (1973, section D), Vaughan et al. (1984, p. 311), and Heidug & Lehner (1985). To derive the condition for phase equilibrium, and to identify the potential to be used in kinetic relations, these authors use only the interfacial balances of mass, momentum, and energy, together with the second law of thermodynamics. Like the Cauchy equation of motion for bulk phases, these results for the interface hold for an arbitrary continuum; application to a specific material requires additional constitutive assumptions. For the special case of an elastic body, equivalent results are derived by Gibbs (1928, pp. 184–196) and by Grinfeld (1981) using Gibbs's principle: At equilibrium, internal energy is minimized, subject to the constraint of constant entropy. Formulating the corresponding minimization problem requires that the state variables be identified; for this reason, the Gibbs approach is applicable only if the solid is elastic.

In these papers, the balance argument is presented either for a specific application (Paterson 1973, Vaughan et al. 1984) or for a particular class of transformation (in the case of Heidug & Lehner 1985, coherent transformation). To free the result from those contexts, we rederive it.

Figure 4 shows the control volume used here. It is fixed in the interface, its faces tangent to the interface have unit area, and its thickness δ normal to the interface is vanishingly small.

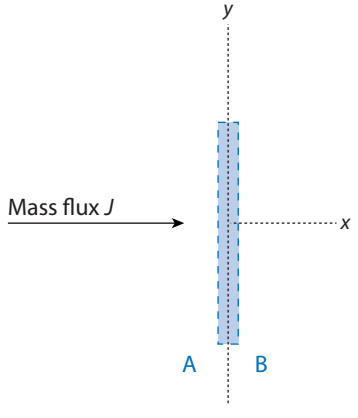

Figure 4

Control volume fixed in the interface.

We use local Cartesian coordinates $\{x, y, z\}$, with x perpendicular to the interface and increasing into the product B. We do not assume plane deformation. Specific energy (internal energy per unit mass), specific entropy, heat flow per unit area in the x direction, temperature, velocity, and specific volume are denoted, respectively, by E, S, q, T, $\mathbf{v}$, and $V = \rho^{-1}$. Temperature is assumed to be continuous; surface energy, negligibly small. For the meaning of the functions E and S of thermodynamic state, in an arbitrary continuum, see Truesdell & Toupin (1960, sections 240, 246, 258). By definition, the mass flux J from parent A to product B is non-negative.

Applied to the matter in the control volume, balances of mass, momentum, and total (internal plus kinetic) energy require that

$$\begin{aligned} \rho^{\mathrm{A}} v_x^{\mathrm{A}} &= \rho^{\mathrm{B}} v_x^{\mathrm{B}} = J, \\ [\sigma_{ix}]_{\mathrm{A}}^{\mathrm{B}} &= 0, \\ J[E]_{\mathrm{A}}^{\mathrm{B}} &= [q]_{\mathrm{B}}^{\mathrm{A}} + [v_i \sigma_{ix}]_{\mathrm{A}}^{\mathrm{B}}. \end{aligned} \qquad (15a,b,c)$$

We interpret Equation 15. Rearranging Equation 15a, we see that $v_x^{\mathrm{A}} = JV_{\mathrm{A}}$ and $v_x^{\mathrm{B}} = JV_{\mathrm{B}}$; conservation of mass requires the normal component v_x of velocity to be discontinuous. Of course, the component u_x of displacement normal to the interface must be continuous. (Assuming otherwise leads to a contradiction: If a void were to open, the pressure within it would drop to the equilibrium vapor pressure, and transformation would cease.) Next, the balance of linear momentum requires the net outflow of momentum to equal the resultant surface force, $J[v_i]_{\mathrm{A}}^{\mathrm{B}} = [\sigma_{ix}]_{\mathrm{A}}^{\mathrm{B}}$; in this form, the momentum balance forms part of the Rankine–Hugoniot relations describing a shock wave. The simplified form (Equation 15b) holds, provided that $|\mathbf{v}|$ is sufficiently small for the momentum flux to be negligible. Last, the first law of thermodynamics requires that $J[E + \frac{1}{2}\mathbf{v}^2]_{\mathrm{A}}^{\mathrm{B}} = [q]_{\mathrm{B}}^{\mathrm{A}} + [v_i \sigma_{ix}]_{\mathrm{A}}^{\mathrm{B}}$: Energy (internal and kinetic) flows out of the volume at a rate balancing the sum of the heat inflow $[q]_{\mathrm{B}}^{\mathrm{A}}$ and the power supplied by the total stress σ_{ij}. Equation 15c follows if $\mathbf{v}^2 \ll 2E$.

In the form of the Clausius inequality (Pippard 1957, p. 94; Truesdell & Toupin, section 258), the second law of thermodynamics requires that

$$[q]_{\mathrm{B}}^{\mathrm{A}} \leq JT\,[S]_{\mathrm{A}}^{\mathrm{B}}. \qquad (16)$$

(Continuity of the absolute temperature T has been used.) In Equation 16, equality holds in the limit as thermodynamic equilibrium is approached; the equation then amounts to the definition of entropy.

Eliminating $[q]_{\mathrm{B}}^{\mathrm{A}}$ between Equations 15c and 16 and then using Equation 15b, we obtain the inequality relating the Helmholtz function $F = E - TS$, the mass flow rate J, and the stress power:

$$J[F]_{\mathrm{A}}^{\mathrm{B}} \leq [v_i]_{\mathrm{A}}^{\mathrm{B}} \sigma_{ix}. \qquad (17)$$

To interpret Equation 17, first consider its implication for transformation occurring arbitrarily close to equilibrium. In this case, the equality holds, and Equation 17 states that if a unit mass is transferred from phase A to B, the increase in Helmholtz free energy (left side of Equation 17) exactly balances the work done by the stress. Farther from equilibrium, the inequality applies in Equation 17. Then the increase in $F = E - TS$ is less because part of the stress power goes to increasing S. This increase in entropy implies that the change of structure occurring across the phase interface is thermodynamically irreversible, even for those transformations in which the transformation strain itself is reversible, as is the case for the coherent transformations described by Equation 2.

To proceed, we must specify the nature of the phase interface. At this point, Vaughan et al. (1984) argue, in effect, that because the olivine–spinel transformation can be induced by applying sufficient hydrostatic pressure at a fixed temperature, one may assume that the shear stress does no work at the phase interface. We return to this assumption in the next section.

With this assumption, the right side of Equation 17 simplifies to $[v_x]^{\mathrm{B}}_{\mathrm{A}}\sigma_{xx} = J[V]^{B}_{A}\sigma_{xx}$. The mass balance (Equation 15a) has been used here. Equation 17 now requires the mass flux J across the interface from A into B to satisfy

$$J[\Phi]^{\mathrm{B}}_{\mathrm{A}} \leq 0, \quad \Phi = F - V\sigma_{xx}. \tag{18a,b}$$

Equation 18 can be satisfied for an arbitrary transformation only if J is a function of $[\Phi]^{\mathrm{B}}_{\mathrm{A}}$. The balance argument thus identifies the potential difference driving rebuilding of the lattice at the interface: Because, as already stated above Equation 15, $J \geq 0$, Equation 18a requires that $\Phi_{\mathrm{A}} \geq \Phi_{\mathrm{B}}$. We see that mass flows from the phase having the higher potential to that having the lower potential. The passage of matter across the interface releases the potential energy difference, allowing it to be used in reconstructing the lattice.

The balance argument provides the interpretation of the potential difference $[\Phi]^{\mathrm{B}}_{\mathrm{A}} = [F]^{\mathrm{B}}_{\mathrm{A}} - \sigma_{xx}[V]^{\mathrm{B}}_{\mathrm{A}}$. The term $[F]^{\mathrm{B}}_{\mathrm{A}}$ represents the increase in stored strain energy (Helmholtz function) as a unit mass crosses the interface; $\sigma_{xx}[V]^{\mathrm{B}}_{\mathrm{A}}$ represents the work done on that mass in compressing it from volume V_{A} to volume V_{B}. If the compression work exceeds the increase in stored energy, then $[\Phi]^{\mathrm{B}}_{\mathrm{A}} < 0$, and mass is converted from A to B. For a hydrostatic stress state, $\sigma_{xx} = -p$; Φ then reduces to the usual Gibbs function (free energy).

General principles require the mass flux J across the interface to be a function of $[\Phi]^{\mathrm{B}}_{\mathrm{A}}$, but do not determine the form of that function. Vaughan et al. (1984) assume the functional form to be the same as that for a hydrostatic stress state; when the potential difference is small compared with the thermal energy, that expression (Turnbull 1956, equation 10.1) can be linearized to give the following (Vaughan et al. 1984, equation 3c):

$$J = -\lambda[\Phi]^{\mathrm{B}}_{\mathrm{A}}. \tag{19}$$

The (positive) rate constant λ depends on T, p, and water concentration; it is a measured quantity, as discussed by Mosenfelder et al. (2001).

In the argument of Vaughan et al. (1984), the only assumption is that the shear stress does no work at the phase interface if the transformation of a sample (possibly a polycrystal) can be induced by purely hydrostatic loading.

6. INTERFACES: COHERENT AND INCOHERENT

In the previous section, we followed Vaughan et al. (1984) in assuming that the shear stress vanishes at the interface. As noted in the discussion of the mass balance (Equation 15a), the normal component of the displacement vector **u** must be continuous across the interface, but there is no such constraint on the component of **u** tangent to the interface. There are two extremes: In continuum mechanics, an interface between phases of identical chemical composition is called coherent if the vector **u** is continuous across it and incoherent if the shear stress vanishes on it (see, e.g, Grinfeld 1981, Truskinovskiy 1984a). In crystallography, the same terms are used in what seems, initially, to be a different sense: As described by, e.g., Christian (1965, section 38), a coherent interface is defined crystallographically as being one across which lattice planes are continuous; an incoherent interface separates phases having no crystallographic relation. Olson & Cohen (1979, p. 1908) argue that the definitions of coherence are consistent; as for the concept of an incoherent interface, they trace it to the work of Nabarro (1940) on precipitation of a

particle of pure metal within the interior of its parent alloy.[2] Because there is no direct evidence that the shear stress vanishes on an incoherent interface, we summarize Nabarro's argument here.

Assuming that elasticity is isotropic and that the lattices of the alloy and the precipitate are identical, so that only change in volume but not shape is involved, Nabarro (1940) reasons as follows: (*a*) For a coherent interface,[3] strain energy is independent of precipitate shape if the shear moduli of the precipitate and the parent are equal; (*b*) a sphere of precipitate cannot form because its strain energy typically exceeds the difference in chemical free energy driving precipitation; (*c*) after considering (and excluding) other possible explanations, Nabarro (p. 530) concludes "the strain can only be effectively released by allowing the precipitate to break away, that is by allowing its lattice to become discontinuous with that of the matrix . . . . The particle recrystallizes in such a way that the shear strain in it vanishes, and only a uniform compression remains." Nabarro (p. 523) gives a physical argument showing that growth of the precipitate particle is accomplished with the minimum increase in strain energy if the shear stress at the interface vanishes.

By extending an argument given by Gibbs (1928, p. 184) in his treatment of the thermodynamic equilibrium of an elastic body in contact with a fluid, Grinfeld (1981) complements the physical argument of Nabarro (1940). Following Gibbs (equation 354), Grinfeld assumes only that, in an elastic body, strain energy per unit volume is uniquely determined by the entropy per unit volume and the components of the deformation gradient. To impose the Gibbs condition that in the state of thermodynamic equilibrium, strain energy is minimized subject to the constraint of fixed total entropy, Grinfeld defines an incoherent interface as being one on which the only constraint is that imposed by mass conservation (as in Equation 15a). Using standard arguments from variational calculus, Grinfeld proves that, at equilibrium, the shear stress indeed vanishes on an incoherent interface (see Grinfeld 1981, equation 2.5). Although his result confirms the physical argument given by Nabarro, both arguments are based on elasticity, and both apply at equilibrium. Nothing in either argument excludes a constitutive equation such as that used to describe grain boundary sliding; in that equation, shear stress at the interface is proportional to the jump in tangential velocity across the interface. Ashby (1972, section 3.2) gives an atomistic model leading to that constitutive relation for a high-angle grain boundary; Christian (1965, p. 332) notes the analogy between a high-angle grain boundary and an incoherent interface.

Although Bos et al. (2005) and Mishin et al. (2010) describe recent work in atomistic modeling of interfaces, I do not know of any attempts to use simulations to test the physical arguments of Nabarro (1940).

7. COUPLING OF LOCAL DEFORMATION TO KINETICS

Motivated by the observation that, in single-crystal tin, melt nuclei first appear when the temperature exceeds by 1–2 K the melting temperature in polycrystalline tin, Lifshitz & Gulida (1952) analyze the coupling between thermodynamics and deformation caused by volume change. In their work, melt is assumed to nucleate as an isolated sphere with a given pressure at infinity; using a composite sphere model, Gulida & Lifshitz (1952) examine the effect of the outer boundary condition, i.e., fixed volume versus fixed pressure.

[2] Lee & Johnson (1978, p. 542) state that "precipitate is stressed in a purely hydrostatic fashion along the precipitate–matric interface." Also, according to Lee et al. (2010, p. 441), "an incoherent precipitate is assumed to be a particle whose interface can support the normal stress but no shear stress."

[3] The words of Nabarro (p. 519) are, "if the lattice of the precipitate remains continuous with that of the matrix."

For the olivine–spinel transformation, the analogous problem is solved by Truskinovskiy (1984b) and Morris (2014). Both authors use a constitutive equation equivalent to Equation 2 and assume that the phases occupy a composite sphere. The sample of parent A is initially at uniform pressure p_0; in the analysis of Morris, the pressure applied to the outer surface of the sample remains at the same constant value p_0, but Truskinovskiy takes the volume of the sample to remain constant as the sample transforms. The configurations also differ: Whereas Truskinovskiy treats growth of a spherical core of product, Morris studies growth of a product rim on a sphere. Because Equation 2 describes a transformation for which the strain is reversible and because the assumption of spherical symmetry implies that the displacement is purely radial, that model does not include the distinction between coherent and incoherent interfaces. This limitation is discussed in the next section. Here, we summarize the properties of the model: Because Equation 2 describes transformations in which the strain is reversible, growth of a core and growth of a rim are equivalent processes if the applied pressure is fixed; within a certain pressure range, a phase can exist metastably; and outside that range, transformation occurs rapidly, on a single timescale set by interface kinetics. The properties described here are obtained by calculating $[\Phi]$ and then equating the rate of mass conversion J to the rate at which the mass of B in the sample increases (Morris 2014, 2017). Properties of the equilibria are obtained by setting $[\Phi]^{\mathrm{B}}_{\mathrm{A}} = 0$; the result is an expression for $[G_0]^{\mathrm{B}}_{\mathrm{A}} = G_0^{\mathrm{B}} - G_0^{\mathrm{A}}$, i.e., the difference between the Gibbs function (free energy) of the phases in the hydrostatic initial state. (The coexistence pressure $\bar{p}$ determined from the Clausius–Clapeyron relation is, as usual, the value of p_0 for which $[G_0]^{\mathrm{B}}_{\mathrm{A}} = 0$.)

These properties are deduced from the model by analysis, but are explained here in physical terms.

7.1. Equivalence of Rim and Core Growth

Figure 5*a*,*b* shows the product B following nucleation; in **Figure 5*b***, rapid nucleation on the sample surface has produced a continuous rim of the type seen in the experiments discussed in Section 4. In **Figure 5*a*,*b***, the volume fraction of phase B is vanishingly small. For the configuration shown in **Figure 5*a***, the phases are in equilibrium across their interface if p_0 is adjusted so that

$$[G_0]^{\mathrm{B}}_{\mathrm{A}} = -\frac{\frac{1}{2}V_0\theta_0^2}{\kappa_{\mathrm{B}} + \frac{3}{4}\mu_{\mathrm{A}}^{-1}}. \tag{20}$$

For further details on this expression, see Morris (2017, equation 21). Truskinovskiy (1984b, equation 6) gives an equivalent result in terms of p_0; also, Morris (2014, equation 27) gives the result for the special case of incompressible phases. For the configuration shown in **Figure 5*b***, the corresponding expression is obtained by replacing μ_{A} in Equation 20 by μ_{B}.

According to Equation 20, for the equilibrium in the configuration shown in **Figure 5*a***, the Gibbs free energy of phase B in the initial hydrostatic state must be less than that of phase A by an amount depending on the rigidity μ_{A} of A; the compressibility κ_{B} of the nucleus; the mean specific volume $V_0 = \frac{1}{2}(V_0^{\mathrm{A}} + V_0^{\mathrm{B}})$; and the fractional difference θ_0 in specific volume, $\theta_0 = (V_0^{\mathrm{B}} - V_0^{\mathrm{A}})/V_0^{\mathrm{A}}$. The subscript 0 denotes a quantity evaluated at the reference pressure p_0. Owing to the spherical symmetry, the mean stress relation (Hill 1963, p. 362) requires that the pressure within the parent phase approach the pressure p_0 applied to the sample surface because, for either configuration, the volume fraction of the product phase is vanishingly small. As a result, the compressibility of the parent phase does not enter into Equation 20. By contrast, because (for spherical symmetry) the deviatoric strain vanishes within the central sphere, independent of the phase occupying it, only the rigidity of the phase within the rim enters into Equation 20. For the configuration in **Figure 5*a***, these two principles explain why analysis yields the expression

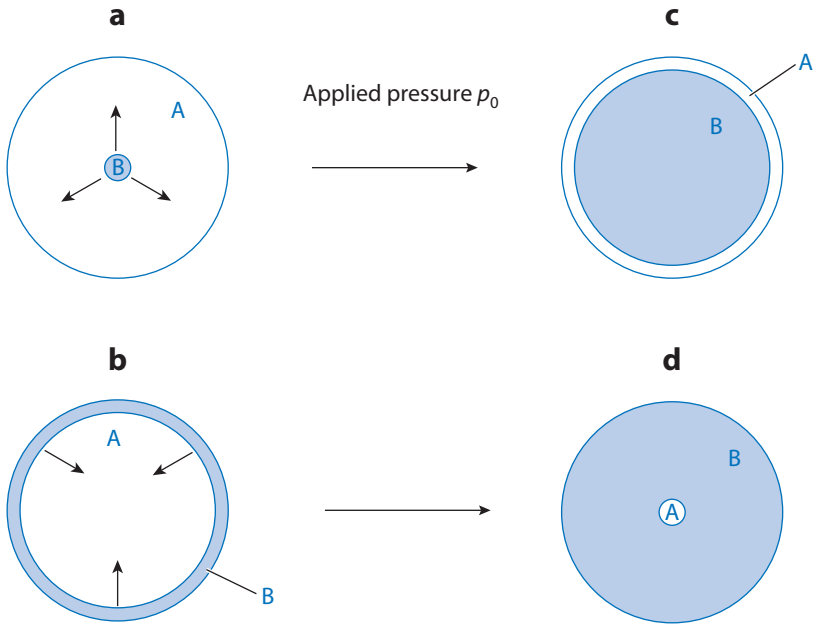

Figure 5

Trivial dependence on configuration of the conditions for A and B to coexist in equilibrium. (*a*,*b*) Configurations in which the volume fraction of product B is vanishingly small: $f_B \to 0$. (*c*,*d*) Configurations in which $f_B \to 1$. As discussed in the text, if B is taken as the dense, high-pressure phase, p_0 must decrease from left to right for the equilibria shown here to exist.

for Equation 20 in which κ_A and μ_B do not appear; they also explain why analysis of rim growth (**Figure 5*b***) yields an expression differing from Equation 20 only in that μ_A is replaced by μ_B.

7.2. Metastability

Figure 5*c* shows the end state in which a vanishingly thin rim of parent A is in equilibrium with product B across their interface. This equilibrium corresponds to

$$[G_0]^B_A = \frac{\frac{1}{2}V_0\theta_0^2}{\kappa_A + \frac{3}{4}\mu_A^{-1}} = -[G_0]^A_B. \qquad (21a,b)$$

According to Equation 21a, for this particular configuration, $[G_0]^B_A > 0$. Because we are always considering A to be the low-pressure phase, $[V_0]^B_A < 0$, so that $[G_0]^B_A > 0$ corresponds to the applied pressure p_0 being less than the Clapeyron pressure $\bar{p}$. To interpret this result, we recall that our model (Equation 2) describes a process in which the strains are reversible. Consequently, one could not tell (even by examining microstructure) whether the material within the thin rim of A had never been transformed or, instead, whether it was newly generated low-pressure product. But in the latter case, we see from the logic used to explain Equation 20 that $[G_0]^A_B$ must be given by Equation 21b.

According to Equation 2, for the configuration shown in **Figure 5*a***, in which A occupies the rim, the A–B transformation occurs over a range of applied pressures p_0, so that

$$-\frac{\frac{1}{2}V_0\theta_0^2}{\kappa_B + \frac{3}{4}\mu_A^{-1}} \le [G_0]^B_A \le \frac{\frac{1}{2}V_0\theta_0^2}{\kappa_A + \frac{3}{4}\mu_A^{-1}}. \qquad (22a,b)$$

In **Figure 5*a***, Equation 22a corresponds to sample density $\rho = \rho_A$ and to $p_0 > \bar{p}$; in **Figure 5*b***, Equation 22b corresponds to $\rho = \rho_B$ and to $p_0 < \bar{p}$. Analysis shows that the model admits a solution in which A and B coexist within this pressure range; according to this solution, the volume fraction f_B of the dense high-pressure product increases as p_0 is decreased (not increased). This behavior is consistent with the end states described by Equation 22. Because the density of the sample as a whole increases with f_B, i.e., from left to right in **Figure 5**, whereas p_0 decreases from left to right, these equilibria existing for $0 < f_B < 1$ correspond to a composite material whose density decreases with increasing pressure. The equilibria are unstable; the composite would separate into regions either of pure phase A or of pure phase B were a sound wave to pass through it. The constitutive relation (Equation 2) describes a material for which there exists a range of pressures in which either phase A or phase B can occupy the entire sample; if that range were entered by increasing p_0, phase A would persist, and otherwise phase B. Within that range, A and B are said to exist metastably. This effect was first predicted by Gulida & Lifshitz (1952).

7.3. Behavior Outside the Metastable Range

If the applied pressure is such that $[G_0]_A^B$ lies outside the range given by Equation 22, the sample transforms completely at a rate determined by interface kinetics (Morris 2017). It is interesting to compare the behavior found in the experiments of Du Frane et al. (2013) on anhydrous samples (<6 ppmw water) with this prediction. According to figure 4*a* of Du Frane et al. (2013), for samples at 18 GPa and 1,273 K, rim thickness grew to about 10 μm within 1 h, but then remained at about that value for up to 6 h (the longest time for which the authors consider their experiments to be unaffected by gain of water). From table 1 of Mosenfelder et al. (2001), we find that at an applied pressure of $p_0 = 18$ GPa at 1,273 K, the difference in the Gibbs free energies for olivine (phase A) and ringwoodite (phase B) is $[G_0]_A^B = -14$ kJ/mol (with an uncertainty of 2 kJ/mol). Using, for the ringwoodite rim, $\mu_B = 126$ GPa, $K_B = 247$ GPa, and $\rho_B = 3.93$ Mg/m^3 (Higo et al. 2008) and, for the olivine core, $K_A = 192$ KPa and $\rho_A = 3.68$ Mg/m^3 (Núñez-Valdez et al. 2013), we find that $|\theta_0| = -0.067$ and $V_0 = 38.6$ cm^3/mol. By Equation 22b, with A and B inverted because B now occupies the rim, the sample should convert completely on a timescale determined by interface kinetics if $[G_0]_A^B \leq -8.63$ kJ/mol. Because the bound in Equation 22b varies as θ_0^2, we note that table 1 of Mosenfelder et al. (2001) does not include values of θ_0. Section 2.3 of Mosenfelder et al. (2001), however, refers to a value of $|\theta_0| \sim 0.08$ (the notation is theirs). For that value, the bound in Equation 22b becomes −12 kJ/mol. For either value of θ_0, the model in Equation 2 predicts that the sample should have transformed completely; the thin and apparently stationary rim observed by Du Frane et al. should not occur.

Although the model is an idealization, the discrepancy at least suggests that further experiments on nominally anhydrous samples at the same temperature but at higher pressure would be of interest. Morris (2017) suggests that the slowing of growth in the anhydrous experiments of Du Frane et al. (2013) could be explained if the rate constant λ decreases in time. Because water is more soluble in ringwoodite than in olivine, the growing rim absorbs water, as shown experimentally by Diedrich et al. (2009); if water is essential to the reconstructive process occurring at the interface, the small amount of water present in the nominally anhydrous samples could be rapidly transferred to the ringwoodite, causing growth to cease.

Peslier & Bizimis (2015) argue that unmetasomatized oceanic lithosphere on the Pacific plate contains less than 50 ppmw of water. This raises the possibility that diffusion of water, rather than heat conduction or rheology, might determine the structure of the metastable wedge. Experiments on the effect of water contents in the range 5–50 ppmw would be of interest.

8. INCOHERENT INTERFACE

As the fourth item in their list of properties exhibited by the olivine–spinel transformation in Mg_2GeO_4, under quasi-hydrostatic stress (stress difference 0.28 GPa), Vaughan et al. (1982) state that spinel grows preferentially in the direction of maximum compressive applied stress. However, at least for the special case of growth of a spherically symmetric rim, the constitutive relation (Equation 2) leads to the prediction that the maximum deviatoric radial strain occurs immediately on the product side of the phase interface (Morris 2014, p. 131). If the product behaved elastically, the corresponding stress would be about an order of magnitude larger than the applied deviatoric stress described by Vaughan et al. (1982). It is not obvious how growth could be correlated with the applied stress field in that case.

This observation by itself suggests that Equation 2 does not correctly describe the reconstructive mechanism occurring when olivine transforms to its spinel phase under quasi-hydrostatic stress. Further, as described in Section 6, the physical picture of Nabarro (1940) implies that, across an incoherent interface of the type observed in the experiments of Vaughan et al. (1982), there is recrystallization, i.e., reconstruction of the lattice across the phase interface. The example of spherically symmetric growth is now particularly instructive: Because, in that problem, the deviatoric strain is zero within the central sphere, the large deviatoric strain occurring immediately on the product side of the interface is generated entirely within the interface itself (Morris 2014, Section 7.1). Once that aspect of the process is recognized, it becomes difficult to believe that the constitutive relationship (Equation 2) can be applicable, even with the addition of creep. Morris (2017) proposes instead that, if the rim behaves elastically, the increment in deviatoric strain subsequent to transformation should be related to the increment in deviatoric stress.

The new constitutive relation is consistent with the observation of Vaughan et al. (1982): Because the deviatoric stress at the interface now vanishes within the product, crystal growth is permitted to respond to whatever external deviatoric stress is present there. Further, when the new constitutive relation is applied to the problem of rim growth, instead of a pressure range in which transformation is prevented (see Equation 22), for any value of $p_0 > \bar{p}$, some transformation occurs. The rim thickness grows to approach a constant value; this value increases with increasing $p_0 - \bar{p}$. The new relation is, at least qualitatively, consistent with the observations of Kubo et al. (1998b); however, when applied to the experiments of Du Frane et al. (2013) on nominally anhydrous samples, it predicts rim thickness about an order of magnitude larger than those observed. This again suggests that, for these experiments, water plays a significant part in controlling rim growth.

Lastly, we note that if the lattice is in fact reconstructed by the transformation, under suitable conditions, dislocation density might actually decrease, rather than increase, as a result of transformation. This idea appears to be experimentally testable.

DISCLOSURE STATEMENT

The author is not aware of any affiliations, memberships, funding, or financial holdings that might be perceived as affecting the objectivity of this review.

LITERATURE CITED

Ashby MF. 1972. Boundary defects and atomistic aspects of boundary sliding and diffusional creep. *Surf. Sci.* 31:498–542

Bhattacharya K. 2003. *Microstructure of Martensite*. New York: Oxford Univ. Press

Bloor MIG, Wilson MJW. 2006. An approximate analytic solution method for the biharmonic problem. *Proc. R. Soc. A* 462:1107–21

Bos C, Sommer F, Mittemeijer EJ. 2005. An atomistic analysis of the interface mobility in a massive transformation. *Acta Mater.* 53:5333–41

Christian JW. 1965. *The Theory of Transformations in Metals and Alloys*. Amsterdam: Pergamon. 1st ed.

Devaux J-P, Fleitout L, Schubert G, Anderson C. 2000. Stresses in a subducting slab in the presence of a metastable olivine wedge. *J. Geophys. Res.* 105(B6):13365–73

Devaux J-P, Schubert G, Anderson C. 1997. Formation of a metastable olivine wedge in a descending slab. *J. Geophys. Res.* 102(B11):24627–37

Diedrich T, Sharp TG, Leinenweber K, Holloway JR. 2009. The effect of small amounts of H_2O on olivine to ringwoodite transformation growth rates and implications for subduction of metastable olivine. *Chem. Geol.* 262:87–99

Dolino G. 1990. The α-inc-β transitions of quartz: a century of research on displacive phase transitions. *Phase Transit.* 21:59–72

Du Frane WL, Sharp TG, Mosenfelder JL, Leinenweber K. 2013. Ringwoodite growth rates from olivine with ~75 ppmw H_2O: Metastable olivine must be nearly anhydrous to exist in the mantle transition zone. *Phys. Earth Planet. Inter.* 219:1–10

Eshelby JD. 1961. Elastic inclusions and inhomogeneities. In *Progress in Solid Mechanics*, Vol. 2, ed. IN Sneddon, R Hill, pp. 89–140. Amsterdam: North-Holland

Frohlich C. 2006. *Deep Earthquakes*. Cambridge, UK: Cambridge Univ. Press

Fung YC. 1965. *Foundations of Solid Mechanics*. Englewood Cliffs, NJ: Prentice-Hall

Gibbs JW. 1928. On the equilibrium of heterogeneous substances. In *Collected Works of J. Willard Gibbs*, Vol. 1, ed. WR Longley, RG Van Name. New York: Longmans, Green and Co.

Green HW. 1986. Phase transformation under stress and volume transfer creep. In *Mineral and Rock Deformation: Laboratory Studies: The Paterson Volume*, ed. BE Hobbs, HC Heard, pp. 201–13. Geophys. Monogr. Ser. 36. Washington, DC: AGU

Green HW, Young TE, Walker D, Scholz CH. 1992. The effect of non-hydrostatic stress on the α–β and α–γ phase transformations. In *High-Pressure Research: Application to Earth and Planetary Sciences*, ed. Y Syono, MH Manghnani, pp. 229–35. Tokyo: Terra Sci./Am. Geophys. Union

Grinfeld M. 1981. On heterogenous equilibrium of nonlinear elastic phases and chemical potential tensors. *Lett. Appl. Eng. Sci.* 19:1031–39

Guest A, Schubert G, Gable CW. 2003. Stress field in the subducting lithosphere and comparison with deep earthquakes in Tonga. *J. Geophys. Res.* 108(B6):2288

Guest A, Schubert G, Gable CW. 2004. Stresses along the metastable wedge of olivine in a subducting slab: possible explanation for the Tonga double seismic layer. *Phys. Earth Planet. Inter.* 141:253–67

Gulida LS, Lifshitz IM. 1952. On the development of local melting nuclei. *Dokl. Akad. Nauk SSSR* 87:523–26

Heaney PJ, Veblen DR. 1991. Observations of the α–β phase transition in quartz: a review of imaging and diffraction studies and some new results. *Am. Mineral.* 76:1018–32

Heidug W, Lehner FK. 1985. Thermodynamics of coherent phase transformations in nonhydrostatically stressed solids. *Pure Appl. Geophys.* 123:91–98

Higo Y, Inoue T, Irifune T, Funakoshi K-I, Li B. 2008. Elastic wave velocities of $(Mg_{0.91}Fe_{0.91})_2SiO_4$ ringwoodite under P–T conditions of the mantle transition region. *Phys. Earth Planet. Inter.* 166:167–74

Hill R. 1963. Elastic properties of reinforced solids: some theoretical principles. *J. Mech. Phys. Solids* 11:357–72

James RD. 1986. Displacive phase transformations in solids. *J. Mech. Phys. Solids* 34:359–94

James RD, Hane KF. 2000. Martensitic transformations and shape-memory materials. *Acta Mater.* 48:197–222

Karato S-I. 2008. *Deformation of Earth Materials.* Cambridge, UK: Cambridge Univ. Press

Kerschhofer L, Dupas C, Liu M, Sharp TG, Durham WB, Rubie DC. 1998. Polymorphic transformations between olivine, wadsleyite and ringwoodite: mechanisms of intracrystalline nucleation and the role of elastic strain. *Mineral. Mag.* 62:617–38

Kirby SH, Stein S, Okal EA, Rubie DC. 1996. Metastable phase transformations and deep earthquakes in subducting oceanic lithosphere. *Rev. Geophys.* 34:261–306

Kohlstedt DL, Keppler H, Rubie DC. 1996. Solubility of water in the α, β and γ phases of $(Mg,Fe)_2SiO_4$. *Contrib. Mineral. Petrol.* 123:345–57

Kolmogorov AN. 1937. On the statistical theory of the crystallization of metals. *Bull. Acad. Sci. USSR* 1: 355–59. Transl. G Lindquist (from Russian), 1992, in *Selected Works of A.N. Kolmogorov*, Vol. 2: *Probability Theory and Mathematical Statistics*, ed. AN Shiryayev, pp. 188–92. Dordrecht, Neth.: Springer

Kubo T, Kaneshima S, Torii Y, Yoshioka S. 2009. Seismological and experimental constraints on metastable phase transformations and rheology of the Mariana slab. *Earth Planet. Sci. Lett.* 287:12–23

Kubo T, Ohtani E, Kato T, Shinmei T, Fujino K. 1998a. Effects of water on the α–β transformation kinetics in San Carlos olivine. *Science* 281:85–87

Kubo T, Ohtani E, Kato T, Shinmei T, Fujino K. 1998b. Experimental investigation of the α–β transformation of San Carlos olivine single crystal. *Phys. Chem. Minerals* 26:1–6

Le Chatelier H. 1890. Sur la polarisation rotatoire du quartz. *Bull. Soc. Fr. Minéral.* 13:119–22

Lee JK, Johnson WC. 1978. Re-examination of the elastic strain energy of an incoherent ellipsoidal particle. *Acta Metall.* 26:541–45

Lee JKW, Tromp J. 1995. Self-induced fracture generation in zircon. *J. Geophys. Res.* 100:17753–70

Lee KM, Lee HC, Lee JK. 2010. Influence of coherency strain and applied stress upon diffusional ferrite nucleation in austenite: micromechanics approach. *Philos. Mag.* 90:437–59

Lifshitz IM, Gulida LS. 1952. On the theory of local melting. *Dokl. Akad. Nauk. SSSR* 87:377–80

Mallard E, Le Chatelier H. 1890. Sur la variation qu'éprouvent, avec la température, les biréfringences du quartz, de la barytine et du disthéne. *Bull. Soc. Fr. Minéral.* 13:123–29

Mishin Y, Asta M, Li Ju. 2010. Atomistic modeling of interfaces and their impact on microstructure and properties. *Acta Mater.* 58:1117–51

Morris SJS. 2014. Kinematics and thermodynamics of a growing rim of high-pressure phase. *Phys. Earth Planet. Inter.* 228:127–43

Morris SJS. 2017. On polymorphic change via an incoherent intermediate state. *Phys. Earth Planet. Inter.* In press

Mosenfelder JL, Connolly JAD, Rubie DC, Liu M. 2000. Strength of $(Mg, Fe)_2SiO_4$ wadsleyite determined by relaxation of transformation stress. *Phys. Earth Planet. Inter.* 120:63–78

Mosenfelder JL, Marton FC, Ross CR, Kerschhofer L, Rubie DC. 2001. Experimental constraints on the depth of olivine metastability in subducting lithosphere. *Phys. Earth Planet. Inter.* 127:165–80

Nabarro FRN. 1940. The strains produced by precipitation in alloys. *Proc. R. Soc. A* 175:519–38

Núñez-Valdez M, Wu Z, Yu YG, Wentzcovitch RM. 2013. Thermal elasticity of $(Fe_x,Mg_{1-x})_2SiO_4$ olivine and wadsleyite. *Geophys. Res. Lett.* 40:290–94

Olson GB, Cohen M. 1979. Interphase-boundary dislocations and the concept of coherency. *Acta Metall.* 27:1907–18

Paterson MS. 1973. Nonhydrostatic thermodynamics and its geologic applications. *Rev. Geophys. Space Phys.* 11:355–89

Peslier AH, Bizimis M. 2015. Water in Hawaiian peridotite minerals: a case for a dry metasomatized oceanic mantle lithosphere. *Geochem. Geophys. Geosyst.* 16:1211–32

Pippard AB. 1957. *Elements of Classical Thermodynamics*. Cambridge, UK: Cambridge Univ. Press

Ringwood AE. 1972. Phase transitions and mantle dynamics. *Earth Planet. Sci. Lett.* 14:233–41

Ringwood AE, Major A. 1970. The system Mg_2SiO_4–Fe_2SiO_4 at high pressures and temperatures. *Phys. Earth Planet. Inter.* 3:89–108

Roitburd AL, Temkin DE. 1986. Plastic deformation and thermodynamic hysteresis in phase transformations in solids. *Sov. Phys. Solid State* 28:432–36

Rubie DC. 1993. Mechanisms and kinetics of reconstructive phase transformations in the Earth's mantle. In *Experiments at High Pressure and Applications to the Earth's Mantle*, ed. RW Luth, pp. 247–303. Edmonton, Can.: Miner. Assoc. Can.

Rubie DC, Karato S, Yan H, O'Neill HStC. 1993. Low differential stress and controlled chemical environment in multianvil high-pressure experiments. *Phys. Chem. Minerals* 20:315–22

Rubie DC, Ross CR. 1994. Kinetics of the olivine–spinel transformation in subducting lithosphere: experimental constraints and implications for deep slab processes. *Phys. Earth Planet. Inter.* 86:223–41

Rubie DC, Tsuchida Y, Tagi T, Utsumi W, Kiegawa T, et al. 1990. An in situ X-ray diffraction study of the kinetics of the Ni_2SiO_4 olivine–spinel transformation. *J. Geophys. Res.* 95(B10):15829–44

Schubnel A, Brunet F, Hilairet N, Gasc J, Wang Y, Green HW. 2013. Deep–focus earthquake analogues recorded at high pressure and temperature in the laboratory. *Science* 341:1377–80

Sokolnikoff IS. 1956. *Mathematical Theory of Elasticity*. New York: McGraw–Hill

Sung C-M, Burns RG. 1976. Kinetics of high-pressure phase transformations: implications to the evolution of the olivine-spinel transition in the downgoing lithosphere and its consequences on the dynamics of the mantle. *Tectonophysics* 31:1–32

Truesdell C, Toupin RA. 1960. The classical field theories. In *Handbuch der Physik*, Vol. III/1: *Principles of Classical Mechanics and Field Theory*, ed. S. Flügge, pp. 226–858. Berlin: Springer

Truskinovskiy LM. 1984a. The chemical potential tensor. *Geochem. Int.* 21:22–36

Truskinovskiy LM. 1984b. The equilibrium between a spherical nucleus and the matrix in a solid-state transformation. *Geochem. Int.* 21:14–18

Turnbull D. 1956. Phase changes. *Solid State Phys.* 3:226–306

Vaughan PJ, Green HW, Coe RS. 1982. Is the olivine–spinel transformation martensitic? *Nature* 298:357–58

Vaughan PJ, Green HW, Coe RS. 1984. Anisotropic growth in the olivine–spinel transformation of Mg_2SiO_4 under non-hydrostatic stress. *Tectonophysics* 108:299–322

Annual Review
of Earth and
Planetary Sciences
Volume 45, 2017

Contents

Researching the Earth—and a Few of Its Neighbors
Susan Werner Kieffer 1

The Fascinating and Complex Dynamics of Geyser Eruptions
Shaul Hurwitz and Michael Manga 31

Plant Evolution and Climate Over Geological Timescales
C. Kevin Boyce and Jung-Eun Lee 61

Origin and Evolution of Water in the Moon's Interior
Erik H. Hauri, Alberto E. Saal, Miki Nakajima, Mahesh Anand, Malcolm J. Rutherford, James A. Van Orman, and Marion Le Voyer 89

Major Questions in the Study of Primate Origins
Mary T. Silcox and Sergi López-Torres 113

Seismic and Electrical Signatures of the Lithosphere–Asthenosphere System of the Normal Oceanic Mantle
Hitoshi Kawakatsu and Hisashi Utada 139

Earth's Continental Lithosphere Through Time
Chris J. Hawkesworth, Peter A. Cawood, Bruno Dhuime, and Tony I.S. Kemp 169

Aerosol Effects on Climate via Mixed-Phase and Ice Clouds
T. Storelvmo 199

Hydrogeomorphic Ecosystem Responses to Natural and Anthropogenic Changes in the Loess Plateau of China
Bojie Fu, Shuai Wang, Yu Liu, Jianbo Liu, Wei Liang, and Chiyuan Miao 223

Interface Kinetics, Grain-Scale Deformation, and Polymorphism
S.J.S. Morris 245

Back-Projection Imaging of Earthquakes
Eric Kiser and Miaki Ishii 271

Photochemistry of Sulfur Dioxide and the Origin of Mass-Independent Isotope Fractionation in Earth's Atmosphere
Shuhei Ono 301

Southeast Asia: New Views of the Geology of the Malay Archipelago
Robert Hall 331

Forming Planets via Pebble Accretion
Anders Johansen and Michiel Lambrechts 359

Tungsten Isotopes in Planets
Thorsten Kleine and Richard J. Walker 389

Shape, Internal Structure, Zonal Winds, and Gravitational Field of Rapidly Rotating Jupiter-Like Planets
Keke Zhang, Dali Kong, and Gerald Schubert 419

Effects of Partial Melting on Seismic Velocity and Attenuation: A New Insight from Experiments
Yasuko Takei 447

Origin and Evolution of Regional Biotas: A Deep-Time Perspective
Mark E. Patzkowsky 471

Statistics of Earthquake Activity: Models and Methods for Earthquake Predictability Studies
Yosihiko Ogata 497

Tectonic Evolution of the Central Andean Plateau and Implications for the Growth of Plateaus
Carmala N. Garzione, Nadine McQuarrie, Nicholas D. Perez, Todd A. Ehlers, Susan L. Beck, Nandini Kar, Nathan Eichelberger, Alan D. Chapman, Kevin M. Ward, Mihai N. Ducea, Richard O. Lease, Christopher J. Poulsen, Lara S. Wagner, Joel E. Saylor, George Zandt, and Brian K. Horton 529

Climate and the Pace of Erosional Landscape Evolution
J. Taylor Perron 561

The Rise of Animals in a Changing Environment: Global Ecological Innovation in the Late Ediacaran
Mary L. Droser, Lidya G. Tarhan, and James G. Gehling 593

The Late Heavy Bombardment
William F. Bottke and Marc D. Norman 619

Reconstructing Climate from Glaciers
Andrew N. Mackintosh, Brian M. Anderson, and Raymond T. Pierrehumbert 649

Autogenic Sedimentation in Clastic Stratigraphy
Elizabeth A. Hajek and Kyle M. Straub 681

Errata

An online log of corrections to *Annual Review of Earth and Planetary Sciences* articles may be found at http://www.annualreviews.org/errata/earth